Electronic Supplementary Material

Timothy Twohig, Sylvio May and Andrew B. Croll

Electronic supplementary material for "Microscopic Details of a Fluid/Thin Film Triple Line".

A. Surface Tensions

Surface tensions of the liquids used experimentally were measured using the Wilhelmy method. A rectangular piece of filter paper is suspended partially into the liquid of interest. The liquid surface tension pulls on the paper and the force is measured using a KSV Instruments Minimicro force sensor. The width and thickness of the filter paper can be measured allowing the surface tension to be determined using the Wilhelmy Equation:

$$\gamma = \frac{F}{d\cos\theta}.$$

Where γ is the liquid's surface tension, F is the force on the Wilhelmy Plate from the test liquid, d is the perimeter of the plate, and θ is the angle at which the liquid contacts the plate and is assumed to be zero for a wetting plate. The measured surface tensions for fluids used in our study are presented below.

Liquid	Surface Tension [mN/m]	Error [mN/m]
Water	73	2
Glycerol	62.3	0.6
Silicone Oil	22.1	0.7
Used Glycerol	45.3	0.8

"Used Glycerol" refers to the glycerol that had been used experimentally, and had come into contact with the floating PS or PC. It is believed that this glycerol may also come into contact with the silicone oil during the floating and sample alignment process. The result is a surface tension lower than that of the pure glycerol. It is believed that some component of the oil wets the glycerol surface and therefore lowers the surface tension. The phenomena was also tested by placing a drop of silicone oil on a pure glycerol bath and measuring the surface tension far from the drop after the drop had been allowed time to spread. This second experiment resulted in a surface tension comparable to that of the "used glycerol".

B. Contact Angles

a. Glycerol Drop on Solid Polymer Contact Angle Measured by Drop Profile

Contact angles of liquid droplets on solid substrates were measured directly by imaging the droplet profile from the side. Drops were placed onto silicon wafers spin coated with either PS or PC, and allowed to equilibrate for ~24 hours. Figure 1(a.) is a side profile of an equilibrated drop with a circle fitted to the profile edge, with (b.) showing the angles and measurements .

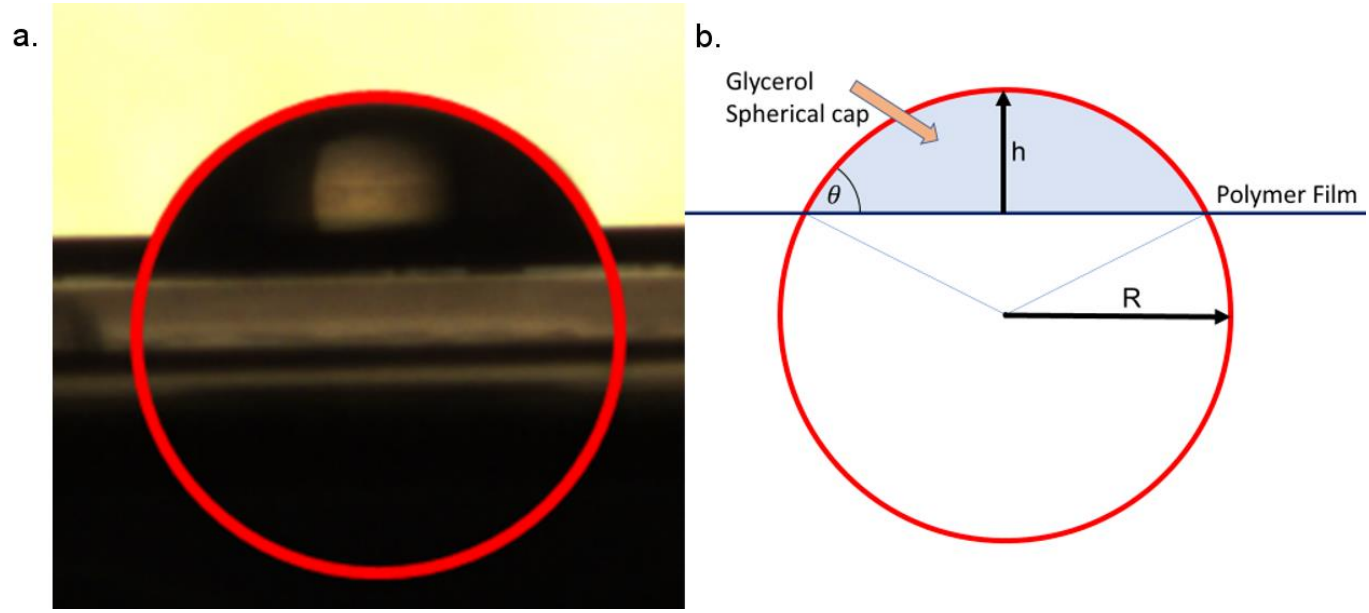

Fig. 1 Picture and schematic of a contact angle measurement using a drop profile. a.) Experimental picture of a spherical glycerol drop resting on a PS substrate, spin-coated onto a silicon wafer. A circle has been fitted to the cap to determine the radius and height of the cap. b.) Schematic of the relevant measurements taken from the drop profile pictures.

A circle was fitted to each drop and the contact angle is determined from the radius of the drop and the height of the spherical cap. The radius (R) and the height (h) of the spherical cap was used to find the contact angle (θ) of the drop,

$$\theta = \arccos\left(1-\frac{h}{R}\right).$$

Receding and advancing angles were created by adding or removing small amounts of fluid to/from the drop, and recording images as soon as possible (usually <10 seconds from change in drop volume) then repeating the removal/addition of liquid and imaging several times in rapid succession (3-4 volume changes). Approximately 20-30 minutes passed after a receding series and the following advancing series. Several hours (2-3) passed between repetitions of the receding/advancing tests. The samples were covered during waiting periods between tests and uncovered for imaging. The results of these tests for pure and used glycerol are presented in the following table.

Materials	Advancing Angle [°]	Receding Angle [°]	Average Angle [°]
Glycerol-PS	77±3.6	65±3.2	71±3.4
Used Glycerol-PS	73±5.7	60±14	67±9.9
Glycerol-PC	63±4.2	57±1.9	60±3.1
Used Glycerol-PC	75±9.0	56±3.0	66±6.0

The contact angles presented here are slightly lower than accepted values for pure materials, possibly due to the use of fluorescent dyes for imaging. The used glycerol had equilibrium contact angles similar to that of the pure glycerol, but the advancing and receding angles were quite different from the pure values as well as variable within the measurement, as represented by the higher error values. Along with the lower surface tension than pure glycerol, this higher variability in advancing and receding angles could be due to the larger effect of pinning of the contact edge from using impure glycerol, leading to stick-slip movements and large jumps in the radius of the liquid drop.

b. Oil Drop on Solid Polymer Contact Angle Measured by Interference

A small droplet of silicone oil was placed onto a flat polymer surface spin coated onto a glass slide and allowed to spread for at least 24 hours, at which point no further spreading was observed. Three-dimensional scans of the edges of the oil droplet were recorded using confocal microscopy. The three-dimensional scans could then be processed to find the height of the peak reflectance intensity for a vertical slice, giving the thickness of the droplet and therefore the contact angle. The interference pattern could also be used to find this shape. The figure below shows the edge of the silicone oil on a solid polymer substrate.

The intensity data from an extracted line could be used to find the coordinates of the peaks and troughs of the interference pattern.

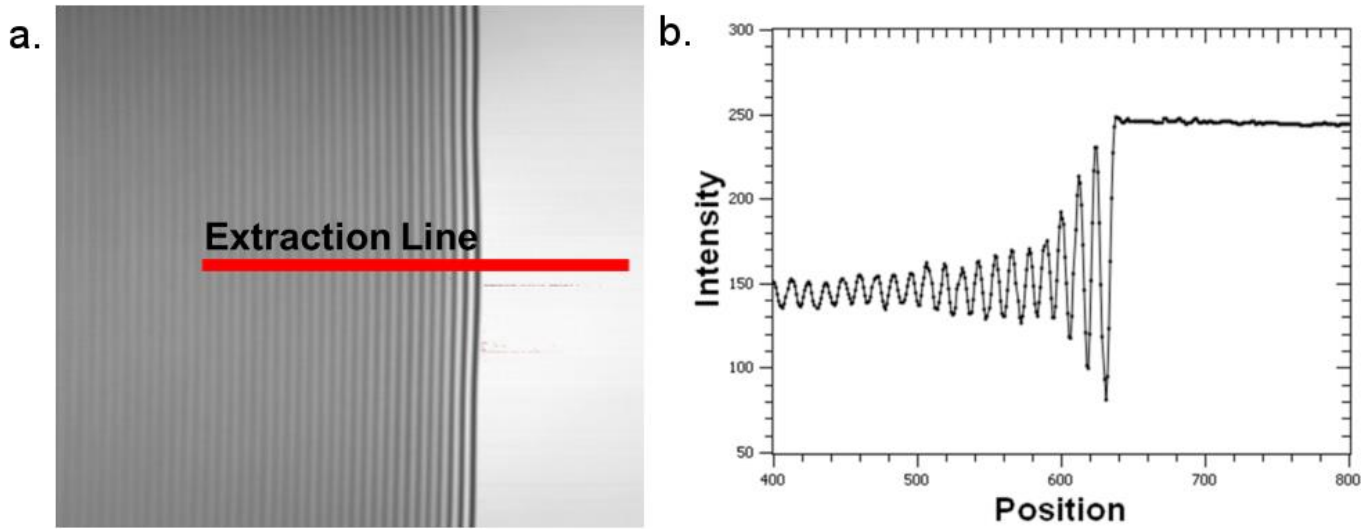

Fig. 2 Interference pattern formed at the edge of an oil drop resting on a PS surface. a.) Constructive and destructive fringes can be seen as well as the line along which the intensity data was extracted. b.) Intensity data for pixels along the extraction line. Peaks and troughs can be seen and correspond to the order of diffraction.

Figure 2 presents the very clear interference pattern and the extracted line which shows the intensity data along the line. The data from this line is presented in (b.) wherein the interference pattern can be seen starting at the droplet edge (position=650) with a destructive interference fringe. The peak intensities of the interference fringes approach a single value as the droplet thickens. The fringes closest to the droplet edge were used with the following equation to find the thickness of the fluid.

$$d = \frac{m\lambda}{2n}$$

The equation above was used to find the height of the surface of the oil, where λ is the wavelength of the laser used, n is the index of refraction of the liquid, d is the thickness of the liquid wedge, and m is the order of the diffraction (m=0.5 is the dark fringe closest to the polymer edge, m=1 is the first bright fringe, m=1.5 is the next dark fringe, etc.). This d -value was added to the heights of the solid polymer surface calculated from the exposed polymer to arrive at the full profile for the solid polymer and the height of the fluid wedge on top. The relative angle between the oil heights and the film surface were then compared to find the contact angle between them. The contact angle values determined from reflectance and interference of opposite sides of the droplet were averaged and are presented in the table below.

Materials	Contact Angle [°]
Silicone Oil-PS	3.2±0.34
Silicone Oil-PC	4.3±0.26

The contact angles for silicone oil on both PS and PC are quite low when compared to liquids such as glycerol or water. These low contact angles indicate that the silicone oil's surface tension allows a great amount of spreading when placed on PS or PC. This behaviour is vastly different from liquids with higher surface tensions that will form much smaller spherical caps with higher contact angles, as observed in Figure 1a above.

C. Film Profiles

Confocal microscopy was used to image the three-dimensional profile of the experimental surfaces. Imaging these surfaces from above allowed the heights of surfaces in air to be determined directly. The polymer film under the glycerol drop was also imaged to obtain the full film profile. However, the image produced was displaced due to the index of refraction of the glycerol. To correct for this, the following equation was used to find the actual film height from the observed film height data:

$$h = d - (d - h_i)n,$$

where h is the actual height of the film, d is the depth of the glycerol drop, h_i is the observed image height, and n is the index of refraction of the glycerol, as shown in Figure 3(a.) along with a height corrected surface profile (b.).

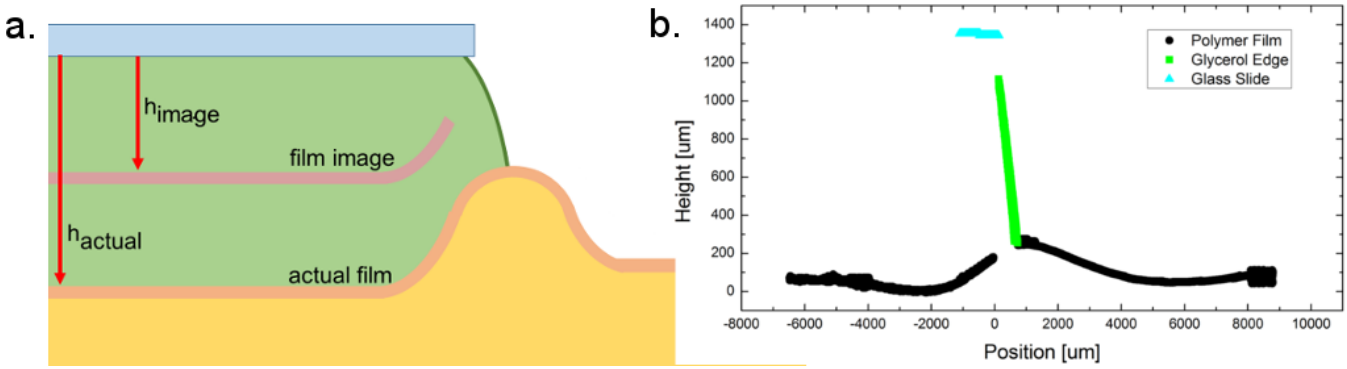

Fig. 3 Side view of data obtained from confocal measurements of the experimental surfaces. a.) The surfaces of the glycerol and polymer in the air are measured directly, but the submerged polymer's image is raised from its actual position. This surface is adjusted to its actual position. This figure is not to scale, the top glass slide is much thinner than the column of glycerol between the slide and the film surface. b.) Experimental surfaces represented on a height vs. position plot. The index-corrected height values for the submerged polymer align with the directly measured film profile.

D. Angle of Glycerol Contacting Film, Measured from Horizontal

The angle at which the glycerol drop approaches the polymer film was measured, with respect to the horizontal for all films presented in the manuscript. The fit procedure is exactly as described in the paper with respect to the angle β. The average results are presented in the table below. The glycerol angles show little or no relation to the thickness of the film they are resting on, with any apparent trend less than the noise in the data of approximately ±10°.

Polymer Used	Average Glycerol Angle	Standard Deviation
PS	71.6	7.2
PC	68.3	8.8

E. Additional angle measurements.

In our work we focus on the angle β because it is directly measured. However, we can also break the measurements down into the subset of θ and ϕ as discussed in the main text. Here we show ϕ for completeness. As expected (because θ is constant) ϕ increases with decreasing thickness as does β.

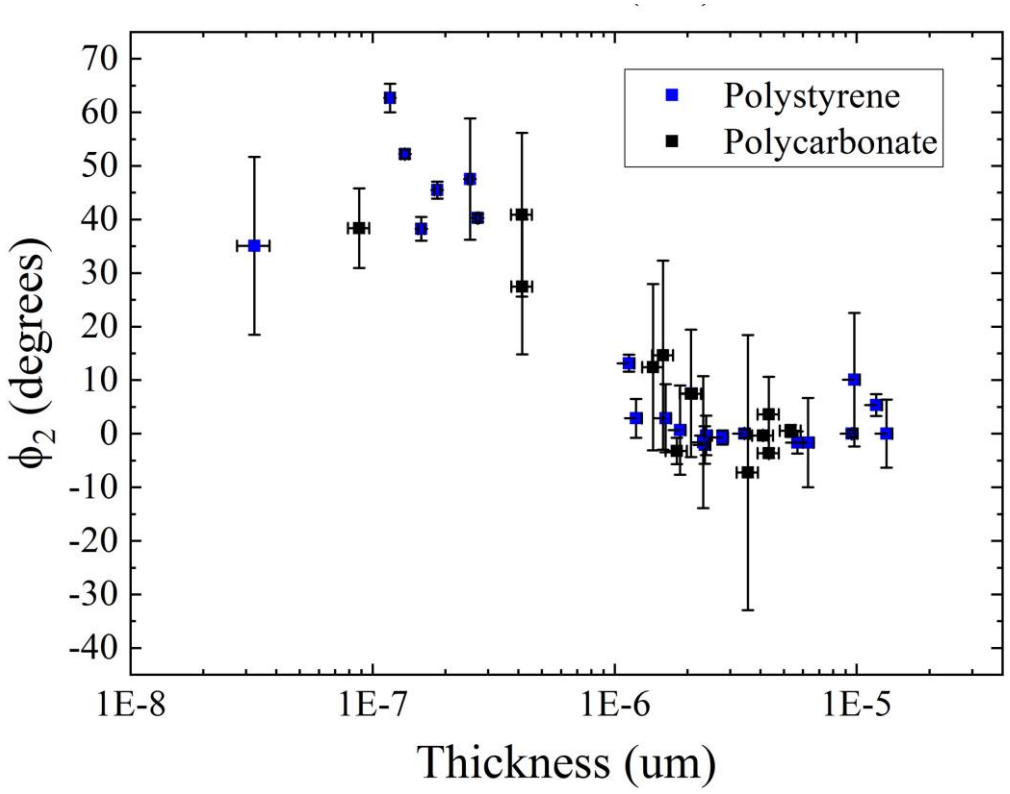

Fig. 4 The angle ϕ_2 as a function of film thickness. Once again PC and PS overlap and show increasing values as film thickness is decreased.

F. Cantilever Beam Example

One of the basic underlying ideas of a fluid/solid triple point is that forces should balance in the vertical and horizontal directions at this point. While this is true, moments must also balance, which destroys any simple symmetry between the direction of the fluid surface or substrate surface and the direction of the forces acting at the triple point. To show that it is not clear that any point on a beam should correlate with the direction of a force applied to the beam, we investigate a cantilever fixed at one end and loaded at the other. In this example forces balance (the beam is not accelerating), however, the direction of the plate surface and applied forces are not related. A model for a beam that represents an unsupported (no gravity) cantilever with a load (P) placed at the end (l) of a beam of width b can be found using the plate equation:

$$EI\, h''''(x)=bP\ ,$$

where $h(x)$ is the vertical position of a beam at length x, E is the Young's modulus of the plate, and $I=\frac{b\,t^3}{12(1-\nu^2)}$ is the second moment of inertia with t as the plate thickness and ν as the plate's Poisson's Ratio (see Figure 4).

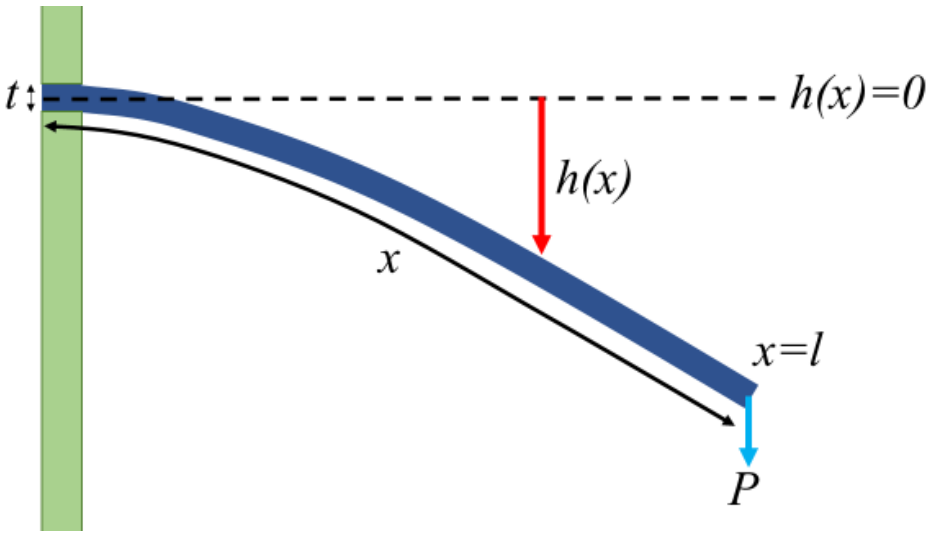

Fig. 5 Schematic of the unsupported cantilever beam described mathematically in this section. The left end of the beam is secured with zero height and zero slope. The negative direction of the load deflects the beam downward.

The sign of the load (P) determines if the beam is deflected up or down. A delta function, $\delta(x-l)$, added to the plate equation allows the load to be added at the end of the beam. Rearranging the plate equation and cancelling the width terms leaves:

$$h''''(x)=\frac{P}{EI}\delta(l-x),$$

where I is now the second moment of inertia per unit width. The boundary conditions imposed are:

$$h'''(l)=\frac{P}{EI},$$
$$h''(l)=0,$$
$$h'(0)=0,$$
$$h(0)=0.$$

Integration and application of the boundary conditions results in the following equations:

$$h'''(x)=\frac{P}{EI},$$

$$h''(x)=\frac{P}{EI}(x-l),$$

$$h'(x)=\frac{P}{EI}\left(\frac{x^2}{2}-lx\right),$$

$$h(x)=\frac{P}{EI}\left(\frac{x^3}{6}-\frac{lx^2}{2}\right).$$

These equations allow the height, slope, and curvature to be found analytically for any part of the cantilever between $x=0$ and $x=l$, where the load is applied. Relevant to our question is the biggest slope in the beam, located at it's end:

$$h'(l)=\frac{P}{EI}\left(\frac{l^2}{2}\right).$$

The slope only becomes infinite (the beam surface parallel to the applied load) if the beam is infinite. Hence for any experimentally attainable values, the beam surface will never be parallel with the applied load.